Soils and Rocks
An International Journal of Geotechnical and Geoenvironmental Engineering
www.soilsandrocks.com
ISSN 1980-9743
ISSN-e 2675-5475

Numerical analysis of laterally loaded barrette foundation

Djamila Behloul[1], Sid Ali Rafa[2], Belkacem Moussai[1#]

Article

Keywords
Barrette foundation
Plaxis 3D
Lateral loading
Barrette nonlinear behavior
Soil constitutive models

Abstract

The effect of soil constitutive models, nonlinearity of the barrette material, loading direction as well as the cross-sectional shape and second moment of inertia on the response the barrette foundation under lateral loading is investigated in this research. The numerical analyses were conducted on a well-documented barrette load test using Plaxis 3D. The investigation results revealed that the response of the barrette is significantly affected by the direction of the applied load and nonlinear behavior of the soil and barrette materials. For rectangular, square, and circular piles with different cross-section areas and same second moment of inertia, the square and circular piles exhibit similar behavior but different from that of the rectangular pile. However, when these piles have the same cross-section area and different second moments of inertia, the behavior of rectangular pile is close to that of square pile when the load is applied along the *x* direction and is close to that of circular pile shape when the load is applied along the y direction.

1. Introduction

The use of foundations with rectangular shape is more advantageous than circular shape, when they have to be designed to resist lateral loads and bending moments in a preferred direction (Ramaswamy & Pertusier, 1986). Wakil & Nazir (2013) performed numerical analyses on barrettes tested in laboratory and indicated that the response of barrettes to lateral loadings depends on the direction of loading and the loading along the major axis resulted in the greatest lateral load capacity. Similar results were reported by Zhang (2003) on lateral barrette load test using FLPIER software.

Most of the published numerical analyses studying the pile behaviour under lateral loading employed the simple elastic model to describe the pile material behaviour [Basu & Salgado (2007), Broms (1964), Choi et al. (2013), Comodromos et al. (2009), Matlock (1970), Poulos (1971), Poulos et al. (2019), etc]. However, the use of this model may lead to an overestimation of the pile lateral capacity, in particular the piles subjected to high rates of loading (Conte et al., 2013).

Choi et al. (2013) reported that rectangular, square and circular cross-sections have similar behaviour under lateral loading when they have the same second moment of inertia, with the assumption that the soil and pile material are to behave as elastic medium.

Poulos et al. (2019) reported that the barrette behaviour can be modelled using equivalent circular pile. An equivalent pile foundation with the same circumference and second moment of inertia as the barrette (in the direction of loading) showed a very similar load-deflection curve.

Siriwan et al. (2020) indicated that the nonlinear concrete model (Schädlich & Schweiger, 2014) captures the deep cement mixing wall failure mechanisms reasonably well compared to Mohr-Coulomb model. Furthermore, the Mohr-Coulomb model overestimates the stability of this type of wall.

This study investigates the effect of some factors such as nonlinearity of the barrette material, barrette cross-sectional shape, second moment of inertia, barrette slenderness, direction of load as well as the soil constitutive models (elastic model, Mohr-Coulomb model and Hardening Soil model) on the behavior of a barrette subjected to horizontal loads using the barrette load test published by Conte et al. (2013) and the software Plaxis 3D.

2. Concrete model

The model takes into account creep, shrinkage, strain hardening (tension and compression), strain softening (tension and compression) as well as strength and stiffness depending on time. Also, it takes into account the non-linearity of the material behavior (Schädlich & Schweiger, 2014). This model was implemented in Plaxis software and was primary used

#Corresponding author. E-mail address: bmoussai@yahoo.ca
[1]University of Science and Technology Houari Boumediene, Civil Engineering Faculty, Algiers, Algeria.
[2]National Center of Studies and Integrated Research on Building Engineering, Algiers, Algeria.

Submitted on February 19, 2022; Final Acceptance on January 9, 2023; Discussion open until May 31, 2023.

https://doi.org/10.28927/SR.2023.002122

This is an Open Access article distributed under the terms of the Creative Commons Attribution License, which permits unrestricted use, distribution, and reproduction in any medium, provided the original work is properly cited.

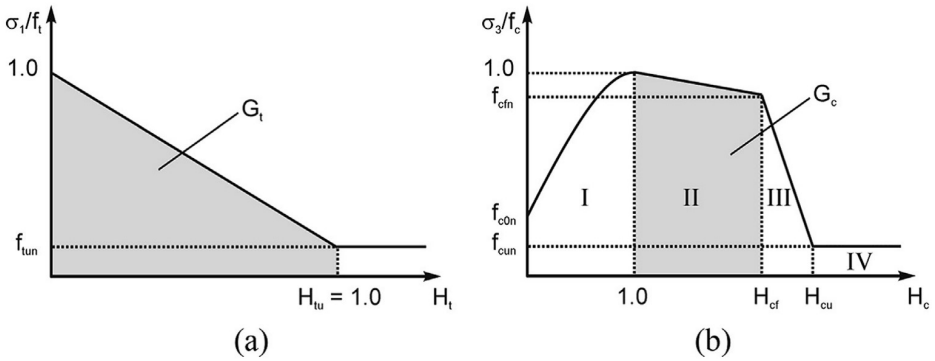

Figure 1. Normalized stress-strain curve in [adapted from Schädlich & Schweiger (2014)]: (a) tension; (b) compression.

to model the shotcrete behavior for tunnels, but it can also be used for other cement-based materials.

The stress-strain curve shown in (Figure 1) includes quadratic strain hardening (I), linear strain softening (II), linear strain softening (III), and constant residual strength (IV). A normalized hardening/softening parameter $H_c = \varepsilon_3^P / \varepsilon_{cp}^P$ is used, with ε_3^P = minor principal plastic strain and ε_{cp}^P = plastic peak strain in uniaxial compression. The input parameters of this model are shown in Table 1.

3. Numerical analysis

Figure 2 shows the barrette load test (Conte et al., 2013) used in the numerical analysis. The barrette cross section is 2.8 m x 1.2 m and its length is 11 m. The barrette cap has a cross-section of 1.5 m x 3.1 m and a thickness of 1.5 m. The barrette embedded in a sandy soil was modelled using nonlinear model for concrete and elastic model for steel reinforcement (Tables 1-2). The Mohr-Coulomb (MC) approach (Brinkgreve et al., 2012) was used to model the soil behaviour.

The subsoil is composed of dense sand with interbedded thin layers of gravel and silty sand. The standard penetration test values vary from 30 to 60. For depths less than 5 m, the cone penetration test values (q_c) vary from 5 to 15 MPa and below this depth, q_c varies from 15 to 30 MPa. Table 3 shows the soil parameters after their calibration by matching the experimental results from the barrette load test with those predicted by the numerical approach on a trial and error basis. Figure 3 shows the model of the barrette load test using Plaxis 3D. The barrette head was subjected to incremental horizontal loads up to 4.6 MPa.

4. Results and discussions

The measured and computed load – deflection curves of the barrette loaded along the major axis is shown in Figure 4a. The results indicated that the computed results using nonlinear model of the barrette concrete is in good

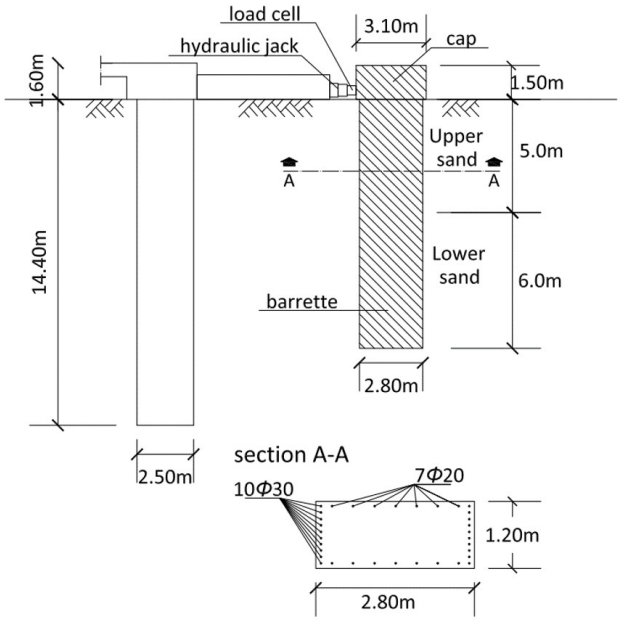

Figure 2. Barrette load test layout (Conte et al., 2013).

Table 1. Input parameters of the nonlinear concrete model.

Parameter	Description	Value
γ (kN/m³)	Unit weight of concrete	25
E_{28} (MPa)	Young's modulus	33600
ν	Poisson's ratio	0.2
$f_{c,28}$ (MPa)	Uniaxial compressive strength	33.2
$f_{t,28}$ (MPa)	Uniaxial tensile strength	3.1
f_{c0n}	Normalized initially mobilised strength	0.1
f_{cfn}	Normalized failure strength (compression)	0.85
f_{cun}	Normalized residual strength (compression)	0.1
ε_{cp}^P	Uniaxial plastic failure strain	-1.20 x10^{-3}
$G_{c,28}$ (kN/m³)	Compressive fracture energy	70
$G_{t,28}$ (kN/m³)	Tensile fracture energy	6.9
ϕ^{MAX}	Maximum friction angle	37

agreement with the barrette load test results. However, the barrette deflections are significantly reduced when the linear model is used.

Figure 4b shows the relationship between the cracking expansion (grey color) and the applied lateral load. When the nonlinear model is used, the tensile strain increases linearly with the applied load until a value of 2.1 MN (initiation of cracking) after which it becomes nonlinear and cracking expands with the increase of load level (Figure 4c).

4.1 Effect of soil constitutive model

The linear elastic, Mohr Coulomb and hardening soil models were used to evaluate their effect on the barrette behaviour. The soil characteristics used in the numerical analysis are given in Table 3.

The results (Figure 5) indicated that the elastic model produces significantly lower deflections than those obtained using Mohr-Coulomb and hardening soil models (HS). As the lateral load increases, the difference in deflections between the three models increases.

Table 2. Properties of the barrette reinforcement steel.

E_s (MPa)	ν_s	F_y (MPa)
210000	0.3	430

The magnitude of the deflection predicted by HS model is slightly lower than that of MC model, especially for higher applied loads. This is because the HS model accounts for stress dependency of the stiffness modulus.

When Mohr Coulomb and hardening soil models are used, the deflection at a load of 4.6 MN is about 6 times greater than that when the linear elastic model is used. This indicates that the linear elastic model significantly underestimates the deflection of the barrette foundation.

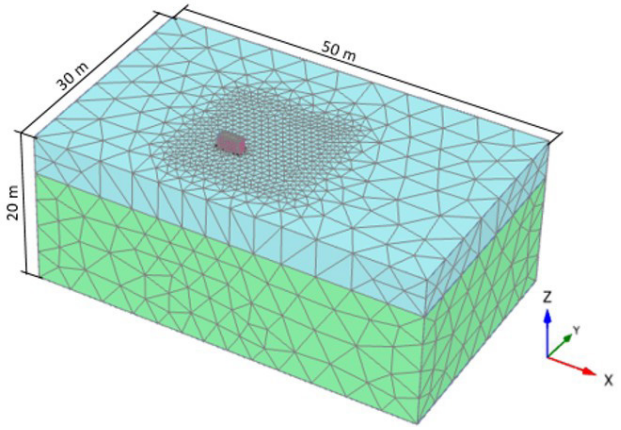

Figure 3. Finite element mesh.

Table 3. Soil parameters.

	Upper sand layer			Lower sand layer		
	Elastic model	Mohr-Coulomb Model	Hardening Soil model	Elastic model	Mohr-Coulomb Model	Hardening Soil model
γ_{unsat} [kN/m^3]	18	18	18	20	20	20
γ_{sat} [kN/m^3]	20	20	20	22	22	22
ν	0.3	0.3	0.3	0.3	0.3	0.3
φ	-	33	33	-	38	38
ψ	-	3	3	-	8	8
E [MN/m^2]	70	70	-	100	100	-
E_{50}^{REF} [MN/m^2]	-	-	70	-	-	100
E_{oed}^{REF} [MN/m^2]	-	-	70	-	-	100
E_{ur}^{REF} [MN/m^2]	-	-	210	-	-	300
ν_{ur}	-	-	0.2	-	-	0.2
m	-	-	0.5	-	-	0.5
R_f	-	-	0.9	-	-	0.9
R_{inter}	0.67	0.67	0.67	0.67	0.67	0.67

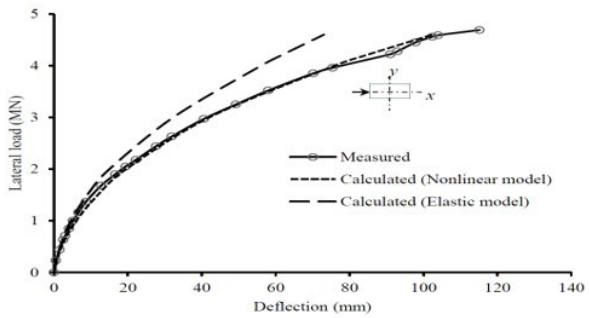

(a)

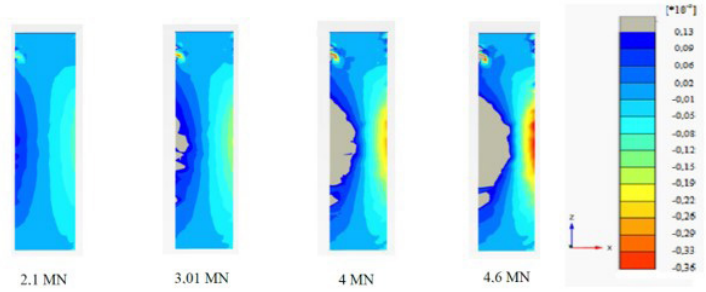

(b)

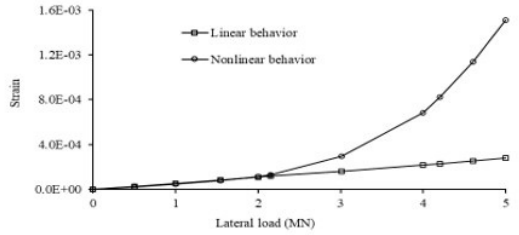

(c)

Figure 4. Results of numerical analyses: (a) measured and predicted load - deflection curves; (b) expansion of cracking (grey color) with increasing load level; and (c) evolution of tensile strain with lateral load level.

4.2 Effect of load direction

Figure 6a shows the deflection of the barrette head when it is loaded along *x* and *y* directions. The results revealed that the deflection of the barrette head is greater along *y* direction than that along *x* direction which may be due to the difference in the barrette moment of inertia about *x* and *y* axes. This result agrees well with those obtained by Zhang (2003) and Wakil & Nazir (2013).

Furthermore, the barrette rotates around its base when the loading is along *x* direction and around a point located above the base when the loading is along *y* direction (Figure 6b-6c).

4.3 Effect of the cross-sectional shape of the foundation

The investigation of the effect of the cross-sectional shape on the barrette behavior was conducted on square

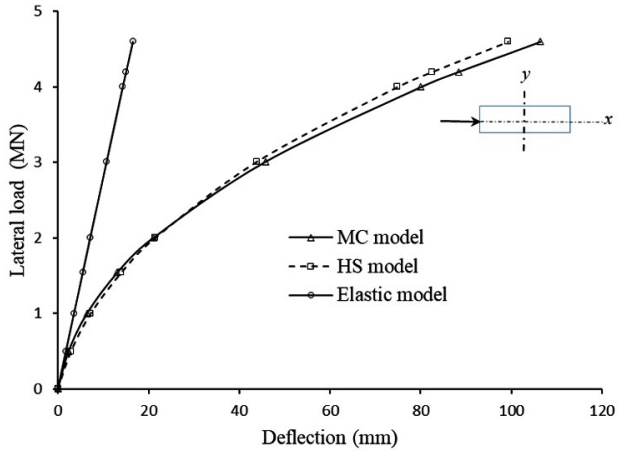

Figure 5. Applied load versus barrette head displacement using Elastic, MC and HS models.

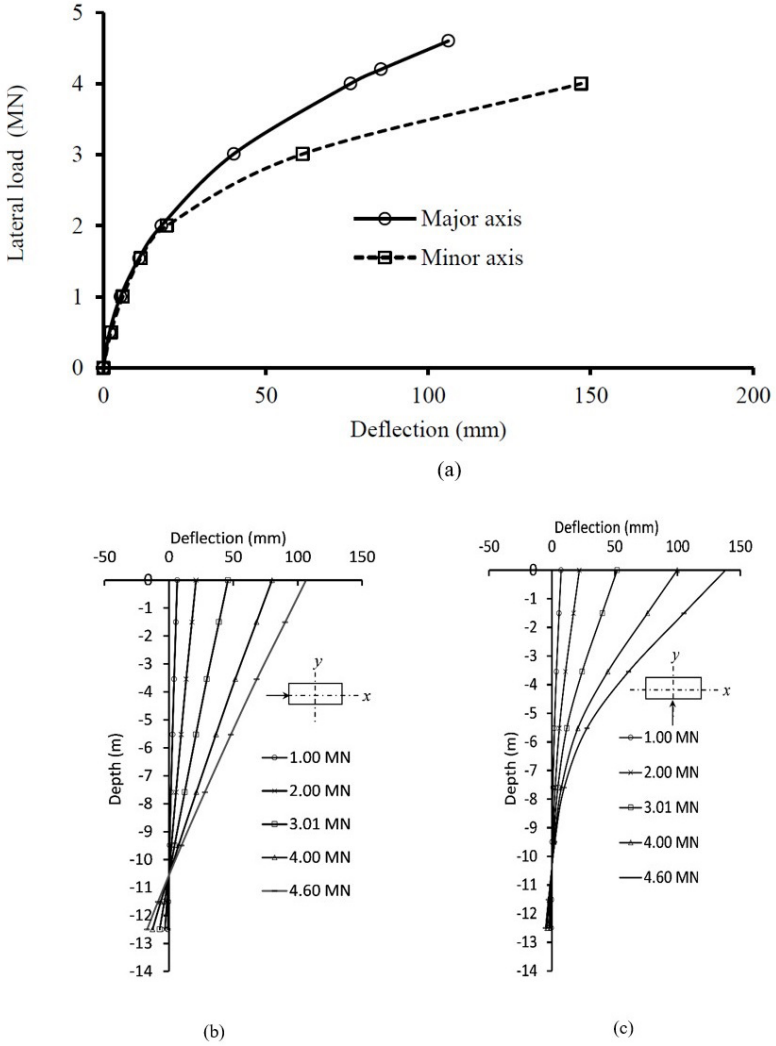

Figure 6. Effects of load direction: (a) applied load versus barrette head deflection along X and Y axes; (b) barrette deflection versus depth along X axis; and (c) along Y axis.

(1.83 x 1.83 m) and circular (2.06 m in diameter) cross-sections having the same cross section area as the reference barrette foundation (i.e. 1.2 x 2.8 m).

The results indicated that (Figure 7), when the applied load is on the major direction (X axis), the rectangular and square shapes showed more resistance than the circular shape. The rectangular and square shapes showed similar behavior until an applied load of about 3 MPa, beyond this load the difference between the two cross-sectional shapes increases as the applied load increases. At the maximum applied load (i.e. 4.6 MPa), the lateral deflection of the rectangular shape is 9% and 33.5% less than that of the square and circular shapes respectively.

However, when the applied load is on the minor direction (Y axis), the rectangular shape resistance is close to that of circular shape and is lower than that of the square shape.

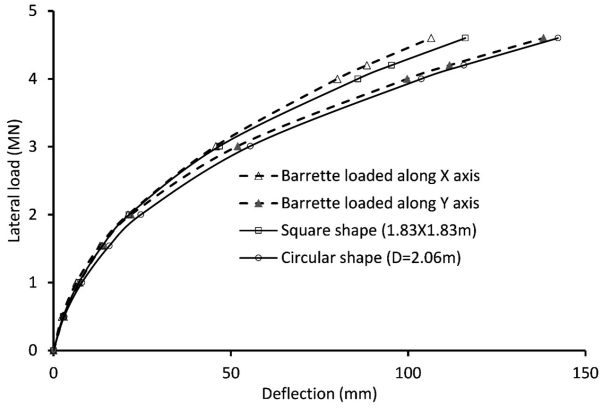

Figure 7. Applied load versus deflection for different cross-sectional shapes of the deep foundation.

4.4 Effect of the second moment of inertia

The analyses were carried -out on square (2.26 m x 2.26 m) and circular (2.54 m in diameter) cross-section shapes having the same second moment of inertia as the barrette foundation loaded along the major axis. The results indicated that the square and circular shapes have similar lateral deflections and are more resistant than the rectangular shape (Figure 8a).

However, when the rectangular barrette foundation is loaded along the minor axis, the square (1.48 m x 1.48 m) and circular (1.69 m in diameter) cross-section shapes having the same second moment of inertia as the rectangular shape, showed similar lateral deflections and less resistance than the rectangular shape (Figure 8b).

Figure 8c shows that the square (1.96 m x 1.96 m) and circular (2.24 m in diameter) shapes are equivalent to the barrette foundation (2.8 x 1.2 m) loaded along the major axis (that is their deflections under lateral loads are similar).

However, the cross- sectional area of the square and circular foundations is more than that of the barrette foundation and therefore, it is more advantageous to use barrette foundation than other pile shapes.

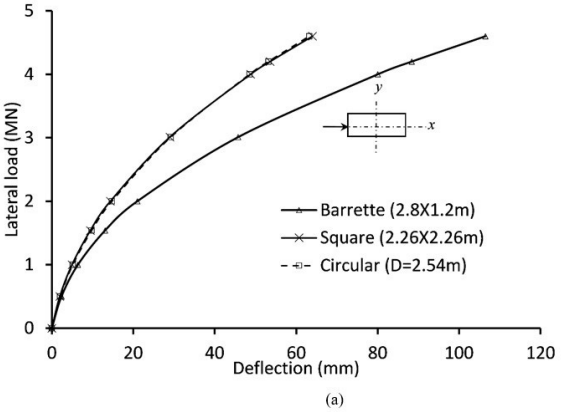

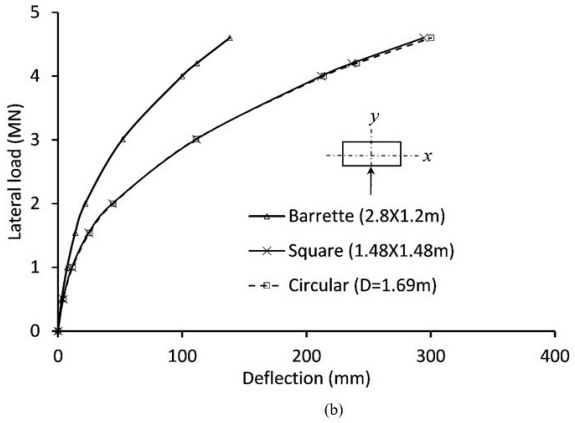

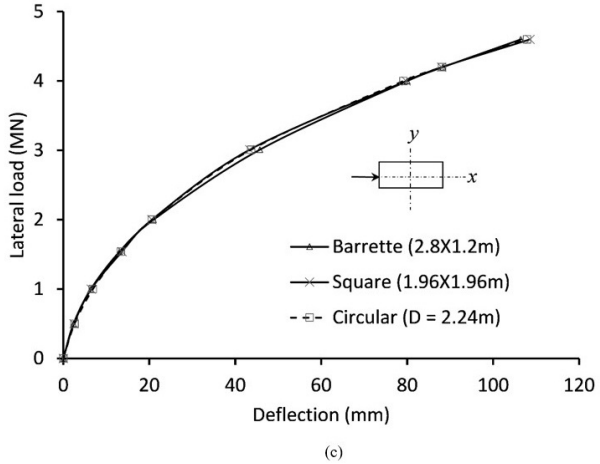

Figure 8. Lateral deflection of square and circular piles, and barrette with different cross-sections and having the same second moment of inertia (a) along X axis and (b) along Y axis, and (c) cross-sections of square and circular piles having the same deflection as the barrette foundation along X axis.

4.5 Effect of the barrette slenderness

In order to investigate the effect of the barrette slenderness, the barrette cross – section width (B) is kept constant and the barrette depth (H) is increased. The analyses were performed with different barrette slenderness (H/B = 5, 10, 15, 20 and 25).

The results show (Figure 9) that the barrette head deflection decreases as the barrette slenderness increases. This effect becomes negligible when the barrette slenderness reaches 15. Furthermore, the barrette rotates around its base when the slenderness is less than 15 and around a point located above the base when the slenderness is more than 15 (Figure 10).

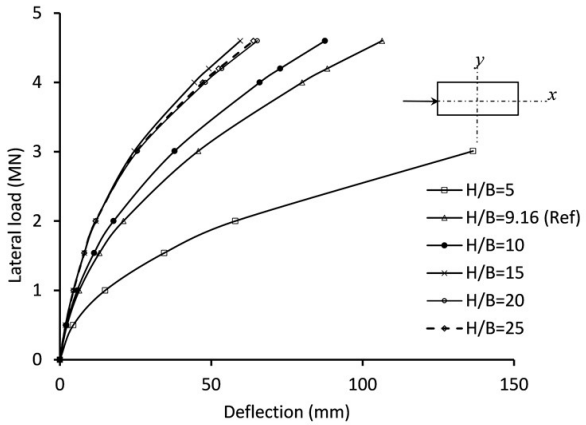

Figure 9. Lateral load versus deflection for different barrette slenderness.

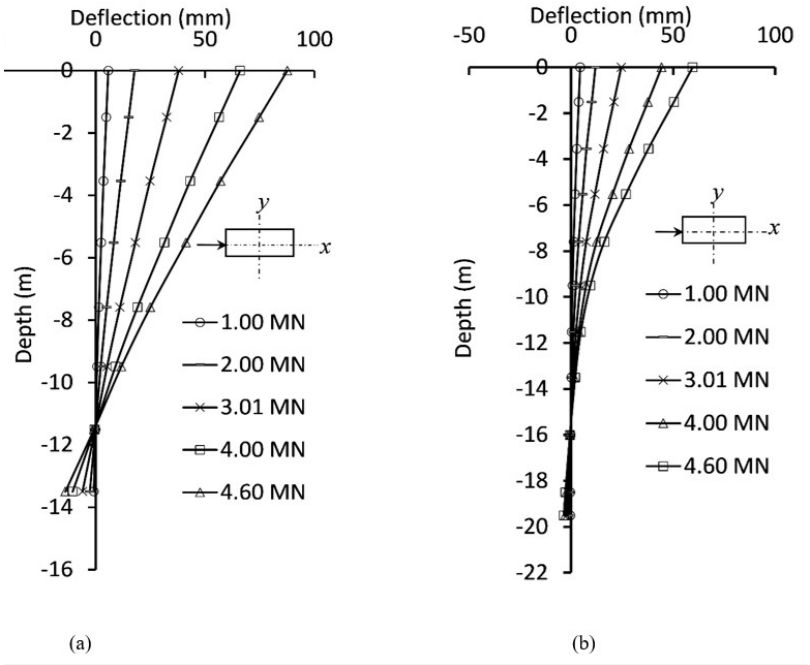

Figure 10. Barrette deflection versus depth for slenderness of (a) 10 and (b) 15.

5. Conclusions

The comparison between measured and predicted load-horizontal displacement curves reveals that the computed results using nonlinear model of the barrette concrete is in good agreement with the barrette load test results. However, the modelling of the barrette material using linear model leads to an underestimation of the barrette horizontal displacements compared to the non-linear model. The horizontal displacement of the barrette head obtained using non-linear model is about 42% more than that obtained using linear model at an applied load of 4.6 MPa.

The resistance of the barrette foundation to lateral loading depends on the direction of the applied load. Its resistance along the major axis is greater than that along the minor axis. Thus, it is more advantageous to use a barrette with rectangular shape loaded on the major direction rather than square or circular shape, especially for high lateral loads.

For foundations with different cross-section shapes and having the same second moment of inertia, their resistance to lateral deflection seems to increase as the width of the foundation in the direction of loading increases.

Declaration of interest

The authors have no conflicts of interest to declare. All co-authors have observed and affirmed the contents of the paper and there is no financial interest to report.

Authors' contributions

Djamila Behloul: conceptualization, methodology, data curation, writing - original draft preparation. Sid Ali Rafa: supervision, methodology, resources, validation. Belkacem Moussai: supervision, validation.

Data availability

The data that support the findings of this study are published by the authors Conte et al. (2013) at https://doi:10.1016/j.compgeo.2012.10.013 and Schädlich & Schweiger (2014) at https://doi.org/10.1201/b17017-20.

List of symbols

$f_{c,28}$: uniaxial compressive strength
$f_{t,28}$: uniaxial tensile strength
f_{c0}: normalized initially mobilised strength
f_{cfn}: normalized failure strength (compression)
f_{cun}: normalized residual strength (compression)
m: amount of stress dependency
q_c: cone penetration resistance
E: Young's modulus of soil
E_{28}: Young's modulus of concrete
E_{50}^{REF}: reference stiffness modulus for primary loading
E_{oed}^{REF}: reference stiffness modulus for oedometer stress-strain conditions

E_s: Young's modulus of steel
E_{ur}^{REF}: reference stiffness modulus for unloading and reloading
F_y: yield strength of steel
$G_{c,28}$: compressive fracture energy
$G_{t,28}$: tensile fracture energy
R_f: failure ratio
R_{inter}: interaction factor
γ: unit weight
γ_{sat}: saturated unit weight
γ_{unsat}: unsaturated unit weight
ε_{cp}^{P}: uniaxial plastic failure strain
v: Poisson's ratio
ϕ: friction angle of soil
ϕ^{MAX}: maximum friction angle of concrete
Ψ: dilatancy angle
ν_{ur}: Poisson's ratio for unloading and reloading

References

Basu, D., & Salgado, R. (2007). Elastic analysis of laterally loaded pile in multilayered soil. *Geomechanics and Geoengineering*, *2*(3), 183-196. http://dx.doi.org/10.1080/17486020701401007.

Brinkgreve, R.B.J., Engin, E., & Swolfs, W.M. (2012). *Plaxis 3D user's manual*. Bentley.

Broms, B.B. (1964). Lateral resistance of piles in cohesionless soils. *Journal of the Soil Mechanics and Foundations Division*, *90*(3), 123-156.

Choi, Y.S., Basu, D., Salgado, R., & Prezzi, M. (2013). Response of laterally loaded rectangular and circular piles in soils with properties varying with depth. *Journal of Geotechnical and Geoenvironmental Engineering*, *140*(4), 04013049.

Comodromos, E.M., Papadopoulou, M.C., & Rentzeperis, I.K. (2009). Effect of cracking on the response of pile test under horizontal loading. *Journal of Geotechnical and Geoenvironmental Engineering*, *135*(9), 1275-1284. http://dx.doi.org/10.1061/(ASCE)GT.1943-5606.0000069.

Conte, E., Troncone, A., & Vena, M. (2013). Nonlinear three-dimensional analysis of reinforced concrete piles subjected to horizontal loading. *Computers and Geotechnics*, *49*, 123-133.

Matlock, H. (1970). Correlations for design of laterally loaded piles in soft clay. In Offshore Technology Conference (Org.), *Proceedings of the 2nd Offshore Technology Conference* (pp. 577-594). Richardson, United States of America: OnePetro. https://doi.org/10.4043/1204-MS.

Poulos, H.G. (1971). Behaviour of laterally loaded piles: I – single piles. *Journal of the Soil Mechanics and Foundations Division*, *97*(5), 711-731.

Poulos, H.G., Chow, H.S.W., & Small, J.C. (2019). The use of equivalent circular piles to model the behaviour of rectangular barrette foundations. *Geotechnical Engineering*, *50*(3), 106-109.

Ramaswamy, S.D., & Pertusier, E.M. (1986). Construction of barrettes for high-rise foundations. *Journal of Construction Engineering and Management*, *112*(4), 455-462.

Schädlich, B., & Schweiger, H.F. (2014). A new constitutive model for shotcrete. In MA Hicks, RBJ Brinkgreve & A Rohe (Eds.), *Numerical Methods in Geotechnical Engineering: Proceedings of the 8th European Conference on Numerical Methods in Geotechnical Engineering* (pp. 103-108). Boca Raton, United States of America: CRC Press. https://doi.org/10.1201/b17017-20.

Siriwan, W., Pornkasem, J., & Schweiger, H.F. (2020). Numerical and experimental investigation of failure of a DCM-wall considering softening behavior. *Computers and Geotechnics*, *119*, 103380. http://dx.doi.org/10.1016/j.compgeo.2019.103380.

Wakil, A.Z., & Nazir, A.K. (2013). Behavior of laterally loaded small scale barrettes in sand. *Ain Shams Engineering Journal*, *4*(3), 343-350.

Zhang, L.M. (2003). Behavior of laterally loaded large-section barrettes. *Journal of Geotechnical and Geoenvironmental Engineering*, *129*(7), 639-648.